

See discussions, stats, and author profiles for this publication at: <https://www.researchgate.net/publication/272190001>

Rapid Evaporative Ionization Mass Spectrometry Imaging Platform for Direct Mapping from Bulk Tissue and Bacterial Growth Media

ARTICLE in ANALYTICAL CHEMISTRY · FEBRUARY 2015

Impact Factor: 5.64 · DOI: 10.1021/ac5046752 · Source: PubMed

CITATION

1

READS

240

10 AUTHORS, INCLUDING:



Abigail Speller

Imperial College London

8 PUBLICATIONS 35 CITATIONS

[SEE PROFILE](#)



James Kinross

Imperial College London

57 PUBLICATIONS 1,871 CITATIONS

[SEE PROFILE](#)



Nima Abbassi-Ghadi

Imperial College London

28 PUBLICATIONS 128 CITATIONS

[SEE PROFILE](#)

Rapid Evaporative Ionization Mass Spectrometry Imaging Platform for Direct Mapping from Bulk Tissue and Bacterial Growth Media

Ottmar Golf,[†] Nicole Strittmatter,[†] Tamas Karancsi,[‡] Steven D. Pringle,[§] Abigail V. M. Speller,[†] Anna Mroz,[†] James M. Kinross,[†] Nima Abbassi-Ghadi,[†] Emrys A. Jones,^{*,†,§} and Zoltan Takats^{*,†}

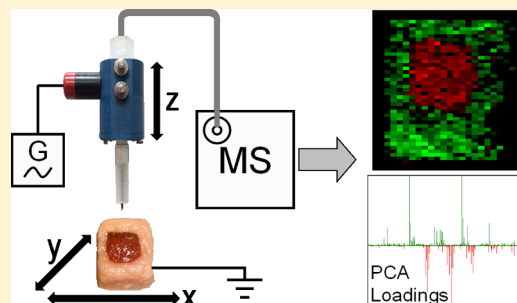
[†]Section of Computational and Systems Medicine, Department of Surgery and Cancer, Imperial College London, SW7 2AZ London, United Kingdom

[‡]Waters Research Centre, HU 1033 Budapest, Hungary

[§]Waters Corporation, SK9 4AX Wilmslow, United Kingdom

Supporting Information

ABSTRACT: Rapid evaporative ionization mass spectrometry (REIMS) technology allows real time intraoperative tissue classification and the characterization and identification of microorganisms. In order to create spectral libraries for training the classification models, reference data need to be acquired in large quantities as classification accuracy generally improves as a function of number of training samples. In this study, we present an automated high-throughput method for collecting REIMS data from heterogeneous organic tissue. The underlying instrumentation consists of a 2D stage with an additional high-precision z-axis actuator that is equipped with an electrosurgical diathermy-based sampling probe. The approach was validated using samples of human liver with metastases and bacterial strains, cultured on solid medium, belonging to the species *P. aeruginosa*, *B. subtilis*, and *S. aureus*. For both sample types, spatially resolved spectral information was obtained that resulted in clearly distinguishable multivariate clustering between the healthy/cancerous liver tissues and between the bacterial species.



Mass spectrometry imaging (MSI) analysis of biological samples allows simultaneous and spatially resolved detection of metabolites, proteins, and lipids directly from biological tissue sections. The technique has gained significant momentum in the course of the last two decades,¹ with the introduction of new techniques such as matrix assisted laser desorption/ionization (MALDI),^{2–4} secondary ion mass spectrometry,^{5–7} and desorption electrospray ionization (DESI).^{8,9} The spatially resolved nature of the resulting data allows its use as a supplemental layer of information for histopathological characterization and classification of tissues,¹⁰ including the possibility of cancer biomarker discovery.^{11,12}

Rapid evaporative ionization mass spectrometry (REIMS)¹³ is a technology recently developed for the real time identification of tissues during surgical interventions. Coupling mass spectrometry with a surgical diathermy device resulted in a technology called the intelligent knife (iKnife), with an intraoperative tissue identification accuracy of 92–100%.¹⁴ The iKnife will potentially improve the oncological outcomes from cancer surgery by ensuring tumor resection margins are free from residual cancer, and it will also minimize the unnecessary resection of healthy tissue. Liver metastases occur in 40–50% of patients with colorectal cancer and determine long-term survival. Surgery for liver metastases has radically improved survival, but a positive resection margin (known as an R1 resection) for surgical treatment of colorectal liver metastases is an important predictor of adverse outcome.¹⁵ REIMS analysis

of biological tissue yields phospholipid profiles showing high histological and histopathological specificity, similarly to MALDI, SIMS, or DESI imaging. Mass spectrometric signal is obtained by subjecting the cellular biomass to alternating electric current at radiofrequency, causing localized Joule-heating and the disruption of cells along with desorption of charged and neutral particles. The resulting aerosol is transported to the mass spectrometer for online mass spectrometric analysis.

In addition to surgical applications, bipolar electrosurgical forceps can also be used for the characterization and identification of intact bacterial cells or cell cultures with no sample preparation.¹⁶ In this process, cellular biomass is held between the tips of the forceps and electric current is applied causing the cells to undergo thermal disintegration and release a partially charged aerosol that is transported to the mass spectrometer. Analysis of 28 clinically relevant microorganisms showed 96%, 98%, and 100% correct identification at the species, genus, and Gram-stain level, respectively.¹⁷ This is of significant importance for the treatment of surgical site infections and sepsis where the rapid detection of bacteria

Received: December 16, 2014

Accepted: February 11, 2015



and their targeted therapy could improve survival and reduce costs and antibiotic resistance.

All REIMS profiling applications require a spectral library of reference mass spectra in order to build the multivariate classification models necessary for pattern-based identification. The collection of iKnife reference mass spectra is currently carried out by manual electrosurgical sampling of ex vivo tissue specimens followed by the histopathological examination of the remaining material. While this workflow provides satisfactory data, there is always significant uncertainty involved at the validation step, since the tissue part producing the spectral data cannot be investigated because it is evaporated in course of the analysis. Hence, all identifications are based on interpolation of the histological environment of the evaporated tissue.

A feasible alternative to manual data collection is the automated, computer-controlled REIMS sampling of tissue specimens, where the 3D tissue environment can be used for histological validation. In principle, a REIMS imaging device can be used in a minimally invasive fashion for the analysis of macroscopic tissue slices (not histological sections) and both the adjacent slice and the remaining tissue material can be fixed, embedded, sectioned, stained, and histologically examined. Although the very cells giving the spectral data are still evaporated, the complete 3-dimensional adjacent environment gives sufficient information about their histological classification. Additionally, the possibility to coregister molecular ion images with optical images of stained sections provides further information about the histological identity of the evaporated cells. Another advantage of computer controlled robotic sampling is the higher precision and reproducibility compared to manual sampling. The main rationale of the current study was to explore this possibility and produce a novel imaging platform for systematic REIMS data collection which can serve as a basis for iKnife applications.

Further motivation for the exploration of REIMS imaging was to develop a mass spectrometric imaging platform for the sample preparation-free, "ambient" imaging MS analysis of biological samples. While DESI and related methods are often referred to as preparation-free analytical approaches, this is certainly not true in the case of tissue imaging. Tissue samples need to be frozen and cryosectioned before analysis, which has a considerable time demand and may also induce chemical changes in the tissues. REIMS, in contrast, does not need any sample preparation (however, the technique is highly destructive), making it an ideal tool for the quick and coarse imaging of arbitrary solid material with biological origin. This area was also explored in the case of bacterial cultures as part of the current study.

■ EXPERIMENTAL SECTION

Sample Treatment and Data Processing. *Sample Treatment.* For the analysis of human samples, ethical approval was obtained from the National Research Ethics Service (NRES) Committee London – South East (Study ID 11/LO/0686). Two samples of fresh human liver containing colorectal adenocarcinoma metastases were obtained from surgical resection specimens and snap frozen to -80°C . Tissue samples were cryosectioned (Thermo Microm HM550 Cryostat, Thermo Fisher Scientific Inc., Germany) to $10\ \mu\text{m}$ thickness and thaw mounted onto glass slides for DESI analysis. The remaining bulk tissue was used for REIMS analysis (workflow is depicted in the Supporting Information, Figure S-1). DESI analysis was carried out using an in-house built DESI

stage, and REIMS analysis was performed using a modified Prosolia flowprobe stage (Prosolia, Inc., USA), which is described in detail later. For more information on DESI and REIMS parameters, see the Supporting Information. REIMS imaging analysis of liver metastasis in cutting mode was carried out at 1 bar Venturi gas pressure, 4 kV p-p amplitude at 50 kHz alternating current frequency (AC), a blade-shaped electrosurgical tip, $500\ \mu\text{m}$ pixel size, 1 mm/s cutting speed, and 1 mm cutting depth. Analysis of liver metastasis in pointing mode was carried out at 0.25 bar Venturi gas pressure, 2 kV amplitude at 50 kHz AC, and with a wire-shaped electrosurgical tip at $750\ \mu\text{m}$ pixel size, 0.1 s time remaining inside the sample, and a pointing depth of 1 mm. REIMS imaging analysis of bacteria was carried out at 1 bar Venturi gas pressure, 2 kV, 40 kHz AC, with a blade-shaped electrosurgical tip, 1 mm pixel size, 0.1 s time remaining inside the sample, and 1 mm pointing depth. Aerosol was transferred with a 1/8 in. OD, 2 mm ID PTFE tubing. Since the used power settings are sufficiently high to cause severe injury, the instrumental setup has to be handled with high caution and according to local health and safety guidance for high voltage systems. Our instrumental setup was developed on the basis of the Health Technical Memorandum 06-03: Electrical safety guidance for high voltage systems (Health and Safety Executive (HSE), UK). Notable safety measures taken in this study included the use of: permanent safety signs, interlocks, electric current limits, insulating gloves, electric isolation and earthing wherever possible, and high voltage indicators on critical parts.

Parameter optimization of the REIMS imaging platform was carried out using porcine liver samples. For comparison of mass spectral patterns between REIMS imaging and iKnife,¹⁴ porcine liver, porcine kidney cortex, lamb liver, and chicken skeletal muscle were analyzed using an electrosurgical handpiece (Meyer-Haake GmbH, Germany) with incorporated PTFE tubing (1/8 in. OD, 2 mm ID) that is connected to the Vernturi pump. Liver, kidney, and muscle were food grade and purchased as such. The iKnife was used in cutting mode at 40 W and 1 bar gas pressure in combination with a Valleylab SurgiStat II power-controlled electrosurgical generator (Covidien, Ireland).

Bacterial strains of *P. aeruginosa* ATCC 27853, *B. subtilis* ATCC 6633, and *S. aureus* ATCC 25923 were cultured in a single Petri dish on solid agar-based media (Oxoid, UK). Incubation was carried out under atmospheric conditions at 37°C overnight. REIMS analysis was carried out directly from solid culture medium on the Waters Xevo G2-S mass spectrometer. Peak identifications were carried out on isolated strains using tandem mass spectrometry and the REIMS bipolar forceps approach.¹⁶

Data Processing. For multivariate image visualization, MS images and optical images were coregistered to define regions of interest (ROIs) for building a supervised training model. On the basis of this model, all other pixels of the slide were classified into the respective classes (healthy/tumor) based on an algorithm that combines recursive maximum margin criterion (RMMC) with linear discriminant analysis (LDA) and is described in detail elsewhere.¹⁸ Further detailed data processing procedures can be found in the Supporting Information.

REIMS Imaging Platform. The REIMS imaging platform consists of three major functional elements that all influence the quality of mass spectra, being the power generator, the xyz-

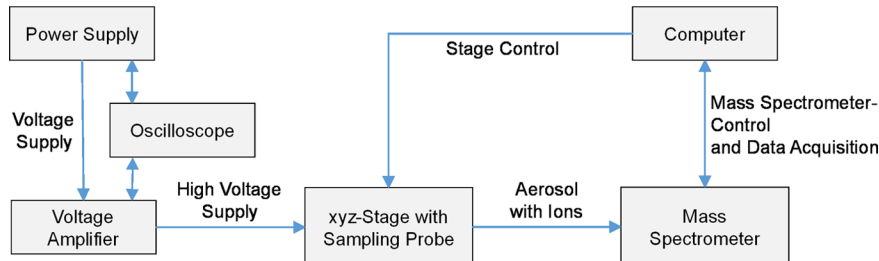


Figure 1. Setup of REIMS imaging instrumentation.

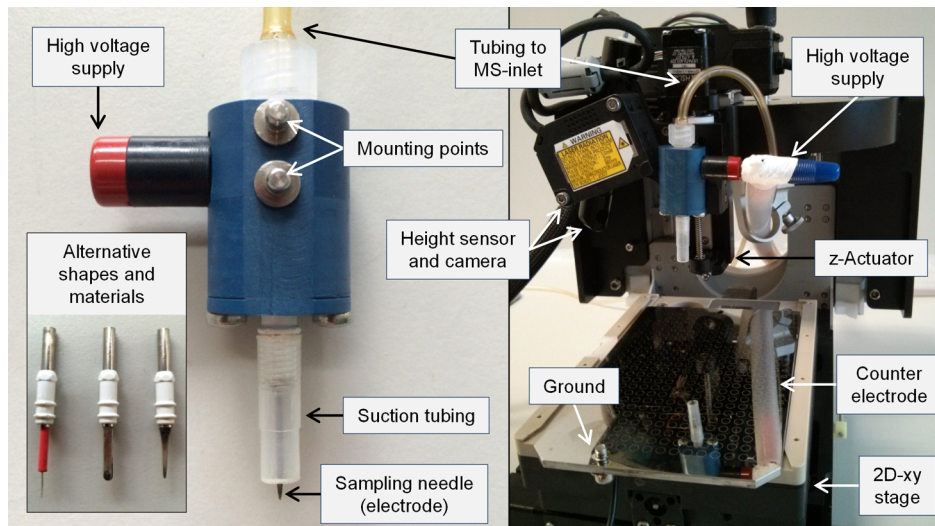


Figure 2. REIMS imaging sampling probe and setup of the *xyz*-stage. The sampling probe is mounted onto the *z*-actuator and is connected to a high voltage power supply. Evaporated aerosol is captured by a suction tubing and transported to the mass spectrometer.

stage with sampling probe, and the mass spectrometer (Figure 1).

The power supply setup used for this platform consists of a Tektronix AFG 3022 arbitrary function generator (Tektronix, Inc., USA), Tektronix DPO 3014 Oscilloscope, and a Trek 10/40A High Voltage Amplifier (Trek, Inc., USA). The arbitrary function generator was used to generate sinus waveforms with amplitudes between 1 and 6 V at frequencies in the range of 10 to 60 kHz. The high voltage power amplifier multiplied the voltage by a factor of 1000 and supplied the connected sampling probe with the electric current. The oscilloscope provided feedback to ensure correct working parameters.

The *xyz*-stage used in the current study is a modified Prosolia 2D DESI stage including Flowprobe upgrade (Prosolia, Inc., USA) with a high precision *z*-axis actuator. The sampling probe is mounted onto the actuator and is connected to the power generator setup as well as the MS inlet capillary (Figure 2). The electrosurgical tip can be exchanged for other materials or shapes depending on the field of application. In the case of high precision sampling, a small diameter wire is advisable, whereas a large surface tip is suitable to maximize mass spectrometric signal intensity. The electrosurgical tip is surrounded by a tubing which is connected to a Venturi air jet pump.

The REIMS imaging platform is capable of two sampling modes: cutting and pointing mode (Figure 3; for videos of both modes, see the Supporting Information media files). In cutting mode, line scans are performed and the electrosurgical tip is kept at a constant *z*-value, while the *x* and *y* values change in a way that a macroscopic cut is made in a right to left trajectory through the tissue, with each subsequent cut made at an

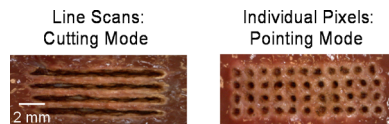


Figure 3. Sampling modes of the REIMS imaging platform.

increment further in the *y* direction. In this approach, the electrosurgical tip is in continuous contact with the sample and therefore continuously producing aerosol. The speed of *x*-movement influences the width of the region of tissue disruption and amount of aerosol produced (Supporting Information, Figure S-3A). If the step size in the *y* direction is smaller than the burning-valley-width, then a complete surface layer is evaporated (Supporting Information, Figure S-3C). In pointing mode, the sampling probe penetrates the sample for a given depth and time. Both factors influence the amount of evaporated aerosol and burn-crater size, similar to the stage movement speed in cutting mode (Supporting Information, Figure S-3B).

In terms of imaging performance, the time of contact between the electrosurgical tip and sample influences the achievable spatial resolution, which is limited by the width of tissue disruption. As ion current is also a function of cutting speed, there is (like in the case of all other MSI methods) a trade-off between spatial resolution, signal intensity, and sampling time. In cutting mode, the speed of imaging depends on a user defined cutting speed, which is usually the already mentioned compromise between mass spectrometer sampling time and desired spatial resolution. In the case of pointing

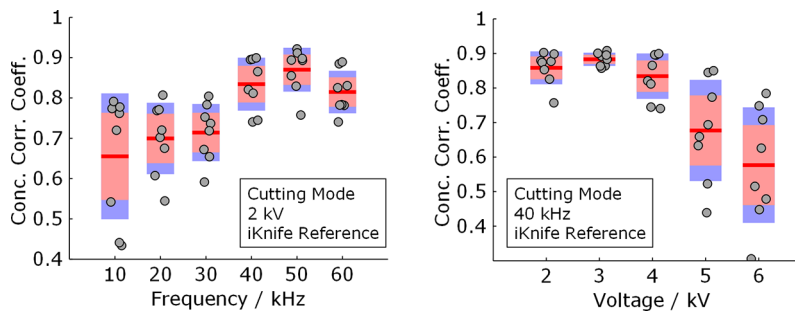


Figure 4. Concordance correlation coefficients between REIMS imaging and iKnife mass spectra in dependency of varying experimental parameters for porcine liver. Red: 1 standard deviation; purple: 1.96 standard deviations (95% confidence interval).

mode, the time necessary to move from one sampling spot to the next is determined by the maximum movement speed of the *xyz*-stage and the time the sampling tip remains inside the sample. In our experiments, the cutting speed was found to be optimal at 1 mm/s and the time necessary to record one pixel in pointing mode was 3 s. Using these parameters, imaging of a 2 × 2 cm sample with 2 mm spatial resolution takes an equal amount of time of about 5 min for pointing and cutting modes (Supporting Information, Table S-1). The additional time necessary to move the *z*-actuator in pointing mode therefore becomes more important if pixel size gets smaller. This leads to a five times higher amount of imaging time at 500 μm pixel size in pointing mode compared to cutting mode. While cutting mode imaging at low resolutions evaporates the whole top sample layer, pointing mode in low resolution leaves the majority of tissue unaffected, allowing the same surface to be characterized at a later time. In both cases, the user of REIMS imaging platform should be aware of the heterogeneity within the sample, as cutting and pointing depth causes tissue evaporation from the bulk sample.

The transfer of aerosol to the mass spectrometer is carried out by using a Venturi air jet pump mounted on the atmospheric interface of the mass spectrometer.¹⁹ The aerosol trajectory is perpendicular to the MS-inlet capillary; thus, larger particles are excluded by momentum separation to avoid clogging and contamination of the mass spectrometer. Excess aerosol was captured by a surgical smoke trap device.

RESULTS AND DISCUSSION

Frequency and Voltage Dependencies. It is critically important that the REIMS imaging platform provides similar ionization conditions as those used in surgery. Commercially available electrosurgical generators used in operating rooms provide highly reproducible mass spectral patterns, which are unique for different histological tissue types.¹⁴ The power supply setup used in the REIMS imaging platform allows variation in amplitude, frequency, and waveform, while an oscilloscope provides feedback ensuring correct working conditions. Depending on the application of the REIMS imaging platform, the experimental parameters can thus be changed to alter ionization conditions and to meet the requirements for recording reference mass spectra for intra-surgical tissue identification or bacterial classification purposes.

The REIMS ionization mechanism is based on Joule-heating,¹⁹ a thermal process, where the heat created is proportional to the square of electric current and the impedance. Depending on the thermal stability of the molecules, thermal degradation may occur as it was observed in the case of phosphatidyl-ethanolamine species which are

partly ionized to both $[M - NH_4]^-$ and $[M - H]^-$, while other phospholipids species form $[M - H]^-$ ions.¹⁹ Therefore, the density and frequency of the electric current have a strong influence on the appearance of the mass spectrum. Electrosurgical generators have an incorporated control loop providing constant power when cutting through tissue, even if the impedance is rapidly changing. This leads to gentle and reproducible cuts with minimized tissue heat exposure. Electrosurgical generators are not easily incorporated into an imaging setup due to a number of safety measures required when used in the operating room, including timing out of the electrosurgical generator after 30 s of continuous use and difficulties accessing the generators electronics. Hence, a simplified power supply was built that offers the freedom to change voltage and frequency parameters and that ultimately allows the creation of mass spectra similar to those obtained by mono- and bipolar electrosurgery. Since a p-p voltage amplitude-controlled RF power supply cannot follow the changing impedance of the sample, it was a critical question as to whether the simplified setup can provide spectra similar to those obtained by using proper electrosurgical equipment.

Optimization of the REIMS imaging platform was carried out by finding the optimal frequency and voltage values to match the iKnife reference mass spectral pattern of porcine liver as shown in Figure 4. Concordance correlation coefficients (CCC)²⁰ were used as a quantitative measure to find the optimal spectral agreement.

In cutting mode, an important factor influencing tissue heat exposure is cutting speed, which leads to high localized temperature for slow speeds and vice versa. Depending on the required ion current, the MS sampling time window needs to be sufficiently long, compromising either spatial resolution or cutting speeds. Therefore, prior to voltage and frequency optimization, a cutting speed needs to be chosen that satisfies requirements on ion yield and spatial resolution. Once a cutting speed is set, heat exposure can be controlled by changing voltage or frequency output of the power generator setup. Cutting speed may need further reiteration, if the available range of voltages and frequencies is not sufficient for adequate heat production. In our study, a cutting speed of 1 mm/s was found to allow gentle cuts at high ion yields.

At a constant p-p voltage of 2 kV, an increase in frequency leads to less thermal degradation and higher similarity to iKnife patterns. According to the oscilloscope readout, the power generator setup was not capable of maintaining a constant increase in power output above 50 kHz at a 2 kV amplitude, explaining the stable CCC between 40 and 60 kHz. At lower frequencies, more in-depth heat dissipation was observed, leading to wide burning valleys, carbonization, and inconsistent

mass spectral patterns with varying baseline noise levels. This was accompanied by strong soot particle production leading to contamination of the MS-inlet capillary, without contributing to the ion yield (Supporting Information, Figure S-4). At higher frequencies (above 40 kHz), visible soot particle production was negligible and no carbonization was observed. This led to mass spectral patterns very similar to those produced by electrosurgical equipment as indicated by CCCs near 0.9. The highest and most consistent TIC was also found to be in that frequency window. An increase in voltage at 40 kHz frequency resulted in similar phenomena as observed with decreasing frequency, such as carbonization and wide burning valleys, leading to high CCCs to be found at low voltages. However, once the voltage was set below 2 kV, ion currents dramatically dropped. This led to an optimal parameter window between 3 and 4 kV and 40 and 50 kHz where CCCs are high and the total ion yield is sufficient.

A similar behavior was observed in pointing mode as it is shown in the parameter optimization plots in the Supporting Information, Figure S-5. A difference between pointing and cutting mode is the time the electrosurgical tip is in contact with the same part of tissue. In cutting mode, the tip is constantly moving and therefore continuously touching fresh tissue, whereas the tip remains at the same tissue spot for a defined amount of time in pointing mode. This leads to longer exposure of heat; thus, voltage and frequency have to be chosen in a way that carbonization is kept at a minimum. At the same time, longer exposure also creates more ions, decreasing the need for higher voltages to gain a sufficiently high TIC. By decreasing the time the tip remained 1 mm inside the sample to a value of 0.1 s, the exposure could be successfully decreased so that the burn crater diameter was 500 μm , while providing good TICs and CCCs at 2 kV and 40 kHz.

The impact of heat exposure on the mass spectral pattern is shown in the Supporting Information, Figure S-6. There is a prominent peak in all mass spectra at $m/z = 885.5$, identified as a phosphatidyl-inositol species [PI(38:4) – H] $^-$. The iKnife reference mass spectrum shows the highest TIC together with the most distinct intensity difference between the PI peak and all other phospholipid signals. The signal-to-noise ratio decreases with increasing voltage, which particularly impacts the spectral pattern in the mass range between m/z 600 and 1000, used for classification. Although the intensity difference between the PI peak and all other peaks is larger for the 2 kV compared to 6 kV spectrum, the TIC of the 2 kV spectrum is lower, indicating a lower level of chemical noise.

Optimized cutting and pointing mode parameters were used to analyze various types of tissues from different animals, including porcine and lamb liver, porcine kidney cortex, and chicken skeletal muscle. Additionally, all samples were analyzed by proper electrosurgical equipment ("iKnife" setup) to ensure selected experimental REIMS imaging parameters are suitable for multiple tissue types. Principal component analysis of the data showed that the overall variance is mostly associated with the tissue types, not the modes of analysis (Figure 5). This is a proof of principle that the experimental parameters are universally applicable to various distinct tissue types in terms of matching the iKnife reference mass spectral patterns. However, larger data sets containing clinically relevant samples are necessary to evaluate the spectral similarity between the three modalities (pointing/cutting/iKnife) in a cross-validated manner. This will be the subject of future research.

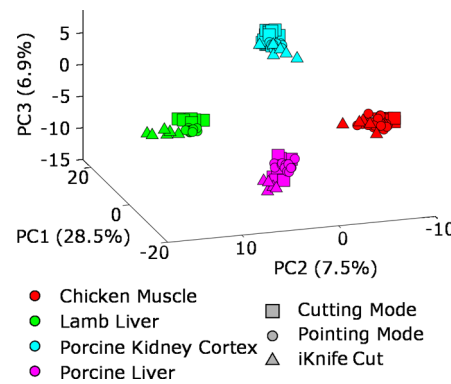


Figure 5. Principal component analysis plot of various kinds of tissue types analyzed with the same experimental REIMS imaging parameters for cutting and pointing mode, respectively.

Imaging. Liver with Metastatic Tumor. The imaging capability of the novel REIMS platform was studied using human liver samples containing colorectal adenocarcinoma metastases (Figure 6). For demonstration of the versatility of the platform, the cutting mode REIMS image was obtained on an Orbitrap instrument, while the pointing mode image was obtained on a time-of-flight mass spectrometer. Supervised multivariate analysis of the tissues revealed a clear distinction between healthy and cancerous tissue for both REIMS imaging and DESI imaging data. The DESI images show a sharp border between the two tissue types as a result of the high spatial resolution and small pixel size of 100 μm . The upper half of the cutting mode REIMS image contains pixels of mixed healthy and tumor pattern influences causing a blurred border. A possible explanation is the direction of the REIMS cut that was performed starting at healthy tissue and continued toward the tumor region. This might have caused the transport of tumor tissue pieces into the healthy area. If these mass spectra ought to be used as reference data for the iKnife, only pixels with a high class-membership probability should be used for training the multivariate models. Unsupervised principal component analysis (PCA) demonstrates high intratissue-type spectral similarity together with spatially distinct clustering of healthy and cancerous data points in PCA space (Supporting Information, Figure S-7). DESI imaging data acquired at high spatial resolution can also be used to locate histological fine structures and their corresponding mass spectra, which can then be coregistered with the REIMS data. The limiting factor for coregistration of DESI and REIMS data is the spatial resolution currently achievable with the REIMS platform. While the cutting mode image was recorded at 500 μm pixel size, the pointing mode image features 750 μm sized pixels. In the case of this liver metastasis sample, the resolution is sufficient; however, in the case of tissues with higher heterogeneity, higher spatial resolution images might be necessary. It is therefore possible that DESI creates a range of different molecular ion patterns coming from the various histological fine structures of heterogeneous tissue, while REIMS is only capable of creating a cumulative molecular ion pattern, representing all histological fine structures at once. A possible solution for an increase in spatial resolution is to decrease the diameter of the electrosurgical tip, which would also be accompanied by lower spectral intensities. However, by connecting the sampling probe directly to the mass spectrometer inlet capillary (as done in the bipolar forceps approach¹⁶), ion yield improves thus overcoming the possible sensitivity issue. This also allows less penetration in the

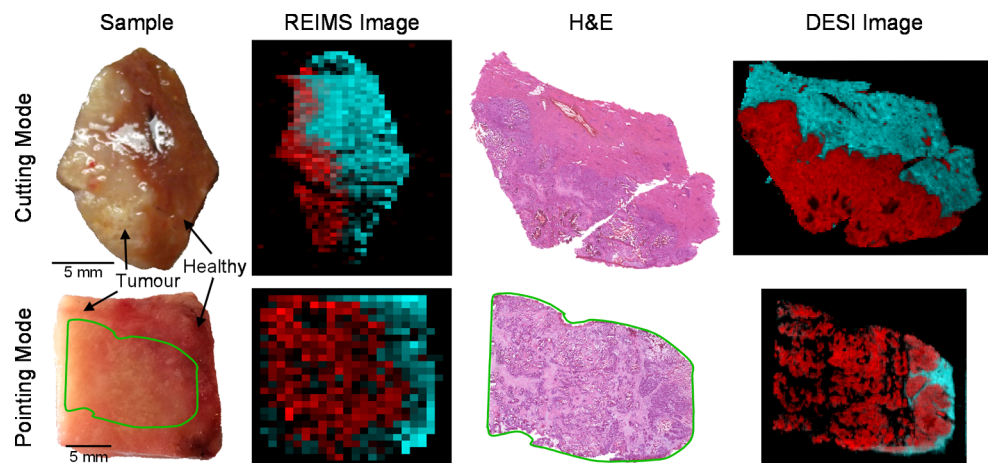


Figure 6. Sample, H&E, and mass spectrometric multivariate images of liver samples with metastatic tumor analyzed by REIMS and DESI. Both techniques clearly differentiate the tissue types. The green border represents the area imaged by DESI.

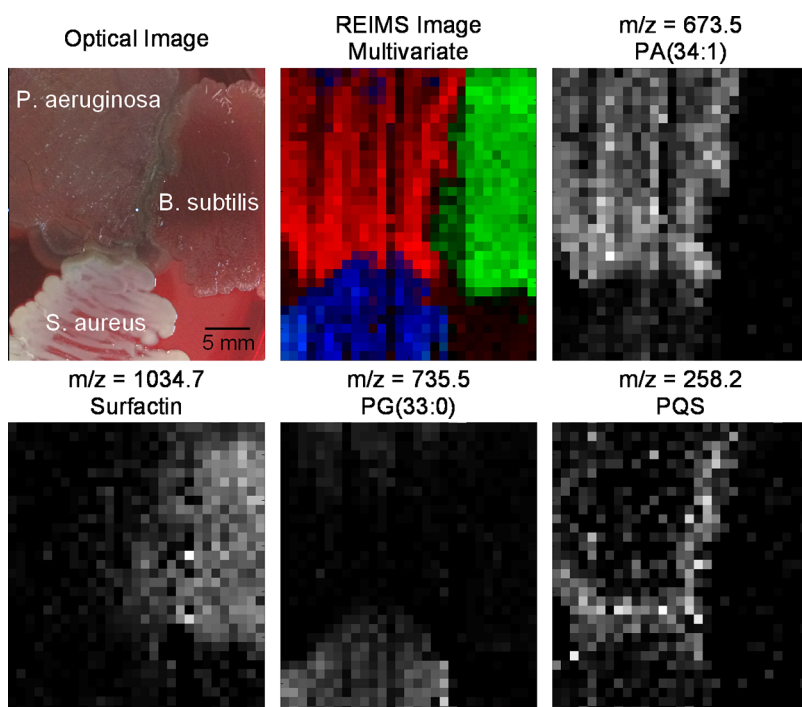


Figure 7. Optical, mass spectrometric multivariate, and ion images of three different bacterial species. The multivariate image shows a clear distinction between the species, while ion images show metabolites of current interest, including phospholipids. Molecules were ionized as $[M - H]^-$. PA: phosphatidic acid; PG: phosphatidyl-glycerol; PQS: 2-heptyl-3-hydroxy-4(1H)-quinolone.

z-direction, decreasing the probability of ionizing unanticipated tissue types. In this regard, improvement in spatial resolution and sensitivity will be the subject of future research.

Multivariate analysis of the liver metastases samples shows a clear distinction of tissue types based on their molecular ion patterns. While REIMS and DESI exhibit different ionization mechanisms resulting in mass spectrometric patterns that are not directly comparable to each other, univariate biochemical comparison of single ions provides a comparable measure for DESI and REIMS coregistration. For certain compounds, the relative intensity difference between two tissue types is similar across all tissue types, ionization techniques, and REIMS analysis modes (cutting and pointing mode). This enables DESI to be used as a fold-change intensity-predictor for REIMS based on up- and down-regulated compounds, which ultimately

represents additional information for unknown tissue type identification. The higher spatial resolution of DESI allows the up- and down-regulated ions to be registered with certain histological features which may not be resolvable by REIMS. This gives insight into the underlying histological composition of a tissue if certain changes in single ion intensities are observed in low resolution REIMS. In the case of metastatic liver comparison, two different phosphatidyl-ethanolamine (PE) species were found to possess opposite relative intensities between healthy and metastatic tissue types as shown in the Supporting Information, Figure S-8. The represented images are RGB color-scale ion images of the two PE ion species. PE(38:4) is more abundant in healthy tissue in all of the REIMS and DESI images, with the REIMS cutting mode image showing barely any presence of this ion in the tumor tissue.

However, compared to the DESI images where this lipid is very abundant even in the tumor tissue, the absence of intensity is likely associated with the overall lower sensitivity achieved by REIMS cutting. An opposite behavior is seen by the ion $[PE(36:1) - H]^-$, showing elevated intensities in the tumor tissue.

Future research will be dedicated to the comparison of multiple samples to obtain cross-validated relative intensity levels for ions of interest. Once enough data is collected, DESI can serve as a biochemical blueprint, allowing tissue types to be histologically annotated with higher confidence when analyzed by REIMS.

Bacteria. Imaging mass spectrometric techniques such as MALDI-MSI and (nano-)DESI-MSI are increasingly applied in microbiological context as they offer the unique opportunity to study the spatially resolved distribution of metabolites in a microbial colony.²¹ Additionally, not only can microbial cultures be studied individually, but also the interactions of different microorganisms can be analyzed directly and in many cases *in vivo* in 2D and after sectioning of the growth medium in 3D.^{22–24} This can reveal novel insights into defense mechanisms of certain types of bacteria and can be extended to the imaging of microbial infections and the study of microbe–host interactions.^{25–27} REIMS imaging analysis of the bacterial strains *P. aeruginosa*, *B. subtilis*, and *S. aureus* was carried out directly from the colonies growing on agar plates *in vivo*. The mass spectra are each dominated by intact phospholipid species in the mass range of *m/z* 600 to 1000, identified as phosphatidic acid (PA), phosphatidyl-glycerol (PG), and phosphatidyl-ethanolamine (PE) species. Fatty acids are mostly present in the lower mass range, whereas cardiolipins give a strong signal in the higher mass range (Supporting Information, Figure S-9). Using the mass range of *m/z* 400 to 2000, all three strains are distinguishable from each other using both supervised and unsupervised multivariate methods (Figure 7 and Supporting Information, Figure S-10). The multivariate image shows distinct separation of each of the three bacterial species and agar. Single ion images reveal the spatial distribution of excreted metabolites such as the lipopeptide surfactin in *B. subtilis*. Surfactin was reported to exhibit antibacterial,^{28,29} antiviral,³⁰ and antifungal³¹ properties. The surfactin signal was equally distributed over the *B. subtilis* culture; however, excretion of surfactin into neighboring areas not directly inhabited by *B. subtilis* can be observed in Figure 7. In the case of *Pseudomonas aeruginosa*, a range of PQS-derived quorum sensing molecules was observed with similar distributions to each other. While structural cell membrane components such as PA(34:1) are equally distributed over the whole area covered by *P. aeruginosa*, the extracellular quorum-sensing metabolites are found in significantly higher abundance on the outer edge of the *P. aeruginosa* growth area as visualized for PQS (Pseudomonas quorum signal, 2-heptyl-3-hydroxy-4(1H)-quinolone) in Figure 7. The area with a high concentration of quorum-sensing molecules seems to correlate to the *P. aeruginosa* bacterial cells that were swarming from the main growth area. Quorum sensing molecules such as PQS are excreted by a wide variety of bacteria for both cell-to-cell communication within the same or between bacterial species.³² Quorum-sensing has been related to a wide variety of behaviors in *P. aeruginosa* including swarming and biofilm production. A comparison of the mean intensity levels of the phospholipid classes shows similar relative intensity distributions for PA, PE, and PG classes across all bacterial strains (Supporting

Information, Figure S-11). The cumulative intensity of PA ion species is slightly elevated compared to the other classes, being approximately 5% higher in intensity compared to the PG class for *P. aeruginosa* and *S. aureus* and about 15% higher for *B. subtilis*.

The results demonstrate successful multivariate differentiation and identification of endogenous and exogenous bacterial species, while simultaneously allowing the spatially resolved localization of metabolic features, eventually giving information on biochemical pathways and interactions between microbial species. A REIMS-based imaging platform additionally marks the first step toward an automated sampling system for microbial cultures for colony-to-colony sampling on a plate containing multiple organisms.

CONCLUSIONS

The automated nature of the REIMS imaging platform enables the systematic collection of reference mass spectra for use in spectral libraries necessary for classification of unknown tissue or bacteria. In both cases, REIMS imaging technology was able to clearly distinguish between healthy/cancerous tissue and between three bacterial strains. This enables the localization of metabolites within the growth area of bacteria as well as an automated identification system for microorganisms.

The ability to arbitrarily choose the material and the shape of the electrode provides a versatile application of the technology depending on the needs of the user, while the availability of two modes of sampling (pointing and cutting) adds another layer of flexibility. Principally, any conductive material with biological origin can be systematically analyzed without prepreparation by this technology, enabling a wide range of applications such as tissue matrix analysis, bacterial identification, or food quality management. Since REIMS mass spectrometric profiles vary across histological tumor types and bacteria, underlying biochemical information enables semiquantitative conclusions to be drawn based on relative intensity distributions of single ions.

ASSOCIATED CONTENT

Supporting Information

Further information on the REIMS imaging workflow, parameter dependencies, plots of multivariate statistical analysis of the presented data, mass spectra, and videos. This material is available free of charge via the Internet at <http://pubs.acs.org>.

AUTHOR INFORMATION

Corresponding Authors

*E-mail: emrys.jones@imperial.ac.uk. Tel: +44 (0) 161 946 2648.

*E-mail: z.takats@imperial.ac.uk. Tel: +44 (0)207 5942760.

Notes

The authors declare no competing financial interest.

ACKNOWLEDGMENTS

This work was supported by the European Research Council under Starting Grant Scheme (Grant Agreement No.: 210356), and Consolidator Grant Scheme (Grant Agreement No.: 185677). Additional support came from the European Commission FP7 Intelligent Surgical Device project (Contract No. 3054940), and the Biotechnology and Biological Sciences Research Council (BBSRC, Reference: BB/L020858/1). We acknowledge Waters Research Centre (Budapest, Hungary)

and Waters Corporation (Wilmslow, UK) for their technical support.

■ REFERENCES

- (1) Van Berkel, G. J.; Pasilis, S. P.; Ovchinnikova, O. *J. Mass Spectrom.* **2008**, *43*, 1161–1180.
- (2) Karas, M.; Bachmann, D.; Bahr, U.; Hillenkamp, F. *Int. J. Mass Spectrom. Ion Processes* **1987**, *78*, 53–68.
- (3) Caprioli, R. M.; Farmer, T. B.; Gile, J. *Anal. Chem.* **1997**, *69*, 4751–4760.
- (4) Spengler, B.; Hubert, M.; Kaufmann, R. In *Proceedings of the 42nd Annual Conference on Mass Spectrometry and Allied Topics*, Chicago, Illinois, May 29 to June 3, 1994; p 1041.
- (5) Liebl, H. *J. Appl. Phys.* **1967**, *38*, 5277.
- (6) Brunelle, A.; Touboul, D.; Laprevote, O. *J. Mass Spectrom.* **2005**, *40*, 985–999.
- (7) Jones, E. A.; Lockyer, N. P.; Vickerman, J. C. *Int. J. Mass Spectrom.* **2007**, *260*, 146–157.
- (8) Takats, Z.; Wiseman, J. M.; Gologan, B.; Cooks, R. G. *Science* **2004**, *306*, 471–473.
- (9) Wiseman, J. M.; Ifa, D. R.; Song, Q.; Cooks, R. G. *Angew. Chem., Int. Ed.* **2006**, *45*, 7188–7192.
- (10) Rompp, A.; Guenther, S.; Schober, Y.; Schulz, O.; Takats, Z.; Kummer, W.; Spengler, B. *Angew. Chem., Int. Ed.* **2010**, *49*, 3834–3838.
- (11) Elsner, M.; Rauser, S.; Maier, S.; Schone, C.; Balluff, B.; Meding, S.; Jung, G.; Nipp, M.; Sarioglu, H.; Maccarrone, G.; Aichler, M.; Ruchtinger, A.; Langer, R.; Jutting, U.; Feith, M.; Kuster, B.; Ueffing, M.; Zitzelsberger, H.; Hofler, H.; Walch, A. *J. Proteomics* **2012**, *75*, 4693–4704.
- (12) Schwamborn, K. *J. Proteomics* **2012**, *75*, 4990–4998.
- (13) Balog, J.; Szaniszlo, T.; Schaefer, K. C.; Denes, J.; Lopata, A.; Godorhazy, L.; Szalay, D.; Balogh, L.; Sasi-Szabo, L.; Toth, M.; Takats, Z. *Anal. Chem.* **2010**, *82*, 7343–7350.
- (14) Balog, J.; Sasi-Szabo, L.; Kinross, J.; Lewis, M. R.; Muirhead, L. J.; Veselkov, K.; Mirnezami, R.; Dezso, B.; Damjanovich, L.; Darzi, A.; Nicholson, J. K.; Takats, Z. *Sci. Transl. Med.* **2013**, *5*, 194ra93.
- (15) Angelsen, J. H.; Horn, A.; Eide, G. E.; Viste, A. *World J. Surg. Oncol.* **2014**, *12*, 127.
- (16) Strittmatter, N.; Jones, E. A.; Veselkov, K. A.; Rebec, M.; Bundy, J. G.; Takats, Z. *Chem. Commun.* **2013**, *49*, 6188–6190.
- (17) Strittmatter, N.; Rebec, M.; Jones, E. A.; Golf, O.; Abdolrasouli, A.; Balog, J.; Behrends, V.; Veselkov, K. A.; Takats, Z. *Anal. Chem.* **2014**, *86*, 6555–6562.
- (18) Veselkov, K. A.; Mirnezami, R.; Strittmatter, N.; Goldin, R. D.; Kinross, J.; Speller, A. V. M.; Abramov, T.; Jones, E. A.; Darzi, A.; Holmes, E.; Nicholson, J. K.; Takats, Z. *Proc. Natl. Acad. Sci. U. S. A.* **2014**, *111*, 1216–1221.
- (19) Schafer, K. C.; Denes, J.; Albrecht, K.; Szaniszlo, T.; Balog, J.; Skoumal, R.; Katona, M.; Toth, M.; Balogh, L.; Takats, Z. *Angew. Chem., Int. Ed.* **2009**, *48*, 8240–8242.
- (20) Lin, L. I. *Biometrics* **1989**, *45*, 255–268.
- (21) Watrous, J. D.; Dorrestein, P. C. *Nat. Rev. Microbiol.* **2011**, *9*, 683–694.
- (22) Yang, Y.-L.; Xu, Y.; Straight, P.; Dorrestein, P. C. *Nat. Chem. Biol.* **2009**, *5*, 885–887.
- (23) Watrous, J.; Hendricks, N.; Meehan, M.; Dorrestein, P. C. *Anal. Chem.* **2010**, *82*, 1598–1600.
- (24) Watrous, J. D.; Phelan, V. V.; Hsu, C.-C.; Moree, W. J.; Duggan, B. M.; Alexandrov, T.; Dorrestein, P. C. *ISME J.* **2013**, *7*, 770–780.
- (25) Liu, W.-T.; Yang, Y.-L.; Xu, Y.; Lamsa, A.; Haste, N. M.; Yang, J. Y.; Ng, J.; Gonzalez, D.; Ellermeier, C. D.; Straight, P. D.; Pevzner, P. A.; Pogliano, J.; Nizet, V.; Pogliano, K.; Dorrestein, P. C. *Proc. Natl. Acad. Sci. U.S.A.* **2010**, *107*, 16286–16290.
- (26) Lane, A. L.; Nyadong, L.; Galhena, A. S.; Shearer, T. L.; Stout, E. P.; Parry, R. M.; Kwasnik, M.; Wang, M. D.; Hay, M. E.; Fernandez, F. M.; Kubanek, J. *Proc. Natl. Acad. Sci. U.S.A.* **2009**, *106*, 7314–7319.
- (27) Moree, W. J.; Phelan, V. V.; Wu, C.-H.; Bandeira, N.; Cornett, D. S.; Duggan, B. M.; Dorrestein, P. C. *Proc. Natl. Acad. Sci. U.S.A.* **2012**, *109*, 13811–13816.
- (28) Vollenbroich, D.; Pauli, G.; Ozel, M.; Vater, J. *Appl. Environ. Microbiol.* **1997**, *63*, 44–49.
- (29) Bais, H. P.; Fall, R.; Vivanco, J. M. *Plant Physiol.* **2004**, *134*, 307–319.
- (30) Kracht, M.; Rokos, H.; Ozel, M.; Kowall, M.; Pauli, G.; Vater, J. *J. Antibiot.* **1999**, *52*, 613–619.
- (31) Sandrin, C.; Peypoux, F.; Michel, G. *Biotechnol. Appl. Biochem.* **1990**, *12*, 370–375.
- (32) Waters, C. M.; Bassler, B. L. *Annu. Rev. Cell Dev. Biol.* **2005**, *21*, 319–346.